

Correlation measurement and group delay tracking in optical stellar interferometry with a noisy detector

T. A. ten Brummelaar

Center for High Angular Resolution Astronomy, Georgia State University

Mon. Not. R. Astron. Soc. **285**, 135-150 (1997)

Abstract

The use of a noisy detector for group delay tracking and/or correlation measurement in optical stellar interferometry is analyzed. Expressions are derived for the signal-to-noise ratio of correlation measurement and the probability of tracking loss in the presence of detector noise. It is shown that such a detector can be suitable for either measurement. For example, the high quantum efficiency of modern CCDs can offset the readout noise to a large extent, making them a good candidate for use in fringe tracking.

1 Introduction

When choosing a detector for optical stellar interferometry many, often conflicting requirements come into play, for example; detector quantum efficiency (DQE), noise, number of pixels, and cost. Ideally, a high DQE, low or even zero noise, multipixel detector is required, and all this at a reasonable cost. A popular detector for interferometry is the avalanche photo diode[1] (APD) which is photon noise limited and, compared to photomultipliers and image intensifiers, has a high DQE. Unfortunately for many tasks, such as group delay tracking (GDT) or multiple band correlation measurement, large numbers of pixels are required. APD's are single pixel devices, and the financial and logistical cost of using them for multi-band observation can be high. Photon noise limited array detectors are available, the PAPA camera[2] for example, although their DQE to date has been rather poor[3]. Cameras based on charge coupled devices (CCD) are now being made with extremely high DQE and relatively low readout noise[4]. The question that then arises is: does the high DQE of the CCD compensate for the addition of readout noise?

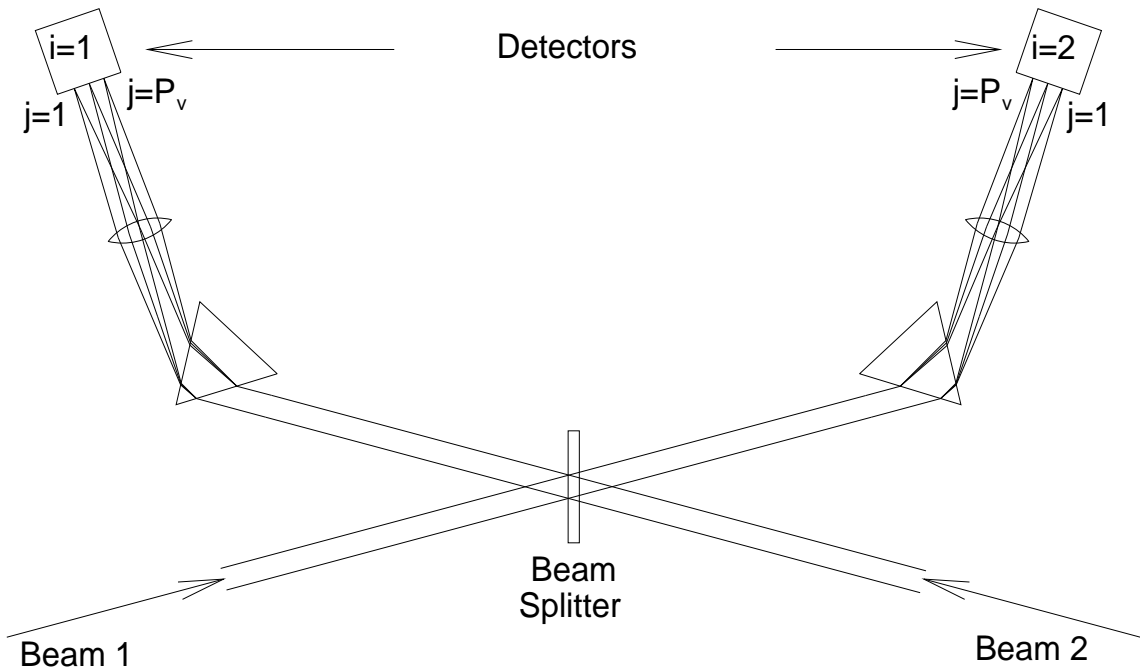


Figure 1: An optical layout for combining two beams. The two beams are combined in the pupil plane using a flat beam splitter. Each output beam is then fed through a dispersive element and imaged onto a detector. With this arrangement there are two separate channels with a fringe phase difference of π radians, labeled $i = 1$ and $i = 2$. Each of these are spread into P_ν wavelength pixels numbered $j = 1, 2, \dots, P_\nu$.

There have been many studies of the effects of photon noise in optical stellar interferometry on fringe correlation measurement[5, 6, 7, 8] and group delay tracking[9, 10]. Except for the work done by Beletic[10] for the Center for High Angular Resolution Astronomy (CHARA) Array[11], all of these assume a photon noise limited detector and ignore the effects of detector noise.

In the analysis that follows, equations are presented for the signal-to-noise (SNR) ratio of correlation measurement as well as for the probability of tracking loss using group delay tracking in the presence of detector noise. Using these expressions, it is demonstrated that it is possible to measure fringe correlation and perform group delay tracking with a noisy detector as long as its DQE is high. In the case of group delay tracking, a CCD would be an excellent choice for a detector. In the case of correlation measurement it is shown that a CCD could be used but may not be the detector of choice. The decision will then come down to logistics and cost considerations. For example, if one already has invested in a highly efficient but noisy detector for fringe tracking, why not also use it for correlation measurement even though it may not be ideal for this application?

2 Fringe and detector model

We will consider a two beam setup for both the case of correlation measurement and fringe tracking. The extension to multiple beams then follows relatively easily. These beams can either be combined in the pupil plane with measurements taken on either side of a beam splitter, or they can be combined in the image plane and viewed on a single array detector. The two methods are equivalent as far as the analysis to follow is concerned[6].

In order to measure the correlation power of a fringe pattern one must modulate the fringe phase in some way. This can be done in a wavelength independent manner by using a beam splitter or by making use of the geometric phase[12]. Alternatively the fringe phase can be changed by modulating the differential path length; either in time by introducing a ramp in the optical path length of each beam, or in space by introducing a differential tilt in the beams. These fringe phase changes are not wavelength independent, however, path length and phase modulations can be treated as equivalent within each narrow spectral channel. For the sake of generality we assume that the fringes are measured on a 2-dimensional array detector where, in one dimension the fringes are spread in phase and in the second dimension they are spread in wavelength. These will henceforth be referred to as the fringe phase dimension and the spectral dimension respectively. An example optical layout can be found in figure 1.

The two beams entering the system are assumed to have been tilt corrected and to have passed through an optical path length equaliser (OPLE) to arrive at the beam combiner with an optical path length difference (OPD) of x meters. Atmospheric effects beyond tilt and residual aberrations due to the optical system are included in a coherence transfer factor η such that the measured visibility magnitude V is given by

$$V(\nu) = \eta |\gamma(\nu)| = \eta_s \eta_t \eta_o |\gamma(\nu)| \quad (1)$$

where $\gamma(\nu)$ is the wavenumber ($\nu = 1/\lambda$) dependent visibility of the object at the current projected baseline, η_s and η_t represent the spatial and temporal effects of the atmosphere and η_o includes the optical system performance. Expressions for the coherence transfer factors for temporal and spatial atmospheric effects can be found in section 5 while the coherence transfer factor for the optical system itself η_o , including any possible high order adaptive optics, can be approximated by the Strehl ratio for the system[13].

The spread in fringe phase across the first dimension of the detector will be written as

$$\Phi_i = \frac{2\pi i}{P_\Phi} s_\Phi(\nu_j) \quad (2)$$

where i is the fringe phase pixel number ranging from 1 to P_Φ and $s_\Phi(\nu_j)$ is the spatial frequency of the fringes formed within the current spectral channel on the detector. In the optical configuration shown in figure 1, there are only two fringe phase pixels in each wavenumber channel, one on each side of the beam splitter, with a wavenumber independent phase difference of π radians. Thus in this case $P_\Phi = 2$ and $s_\Phi(\nu_j) = 1$.

The pixels in the spectral dimension of the detector are arranged evenly in wavenumber ν . This can be done by rebinning the data collected by a detector linear in space, a process that can be performed noiselessly and on-chip in the case of a CCD or by software for a photon counting array detector. Alternatively, one could use a dispersive optical system that directly produces a spectrum linear in space and wavenumber such as a grism[14]. If the pixels in each channel range from wavenumber ν_1 to wavenumber ν_{P_ν} , the central wavenumber of the j th pixel is

$$\nu_j = \nu_1 + (j - 1) \frac{(\nu_{P_\nu} - \nu_1)}{(P_\nu - 1)} \quad (3)$$

where P_ν is the number of pixels across the spectrum. Each spectrum formed in this way will contain channel fringes with a spatial frequency directly related to the OPD $x(t)$ via

$$s_\nu(t) = x(t)(\nu_{P_\nu} - \nu_1) \quad (4)$$

which is the basis of group delay tracking to be discussed in section 4.

We now write the light intensity measured in the pixel representing the i th fringe phase ($1 \leq i \leq P_\Phi$) and the j th wavenumber ($1 \leq j \leq P_\nu$) as

$$I_{ij}(t) = I_0 \times \left[1 + V(\nu_j) \cos \left(\underbrace{\frac{2\pi i}{P_\Phi} s_\Phi(\nu_j)}_{\text{Phase Term}} + \underbrace{\frac{2\pi j}{P_\nu} s_\nu(t)}_{\text{Spectral Term}} + \underbrace{\Phi(t)}_{\text{Other Terms}} \right) \right] \quad (5)$$

where I_0 is the expected classical intensity from both apertures in a single pixel including the atmosphere and optical system performance and

$$\Phi(t) = 2\pi\nu_1 x(t) + \Phi_\gamma(\nu_j) + \Phi_{\text{atm}}(t, \nu_j). \quad (6)$$

The quantity $\Phi_\gamma(\nu_j)$ is the visibility phase at the wavenumber ν_j , and $\Phi_{\text{atm}}(t, \nu_j)$ is the phase difference introduced by atmospheric turbulence. This intensity pattern is sampled by the detector at a sample time τ which will be of the order of the temporal coherence time of the atmosphere τ_0 .

All of the quantities in the cosine function in equation (5) depend on the wavenumber ν_j and so the two dimensions of the detector are not independent. In all of the analysis to follow we will therefore either be making a measurement within a single wavenumber channel, in the case of a fringe correlation measurement, or across a single fringe phase channel, in the case of a fringe tracking measurement.

We are now in a position to write an expression for the expected number of counts measured in a given pixel during a single sample period. The count of photon events in the pixel representing fringe phase Φ_i and wavenumber ν_j during sample period k is written

$$n_{ijk} = c_{ijk} + r_{ijk} \quad (7)$$

where c_{ijk} is the signal term and r_{ijk} is the noise term. The signal c_{ijk} follows Poisson statistics with an expectation value of

$$\langle c_{ijk} \rangle = N \times \left[1 + V(\nu_j) \cos \left(\frac{2\pi i}{P_\Phi} s_\Phi(\nu_j) + \frac{2\pi j}{P_\nu} s_\nu(k\tau) + \Phi(k\tau) \right) \right]. \quad (8)$$

Here, N is the expected photon count corresponding to an intensity of I_0 taking into account the quantum efficiency of the detector. One must be careful about the definitions of N and V , especially when comparing expressions for SNR in the literature, as they vary from paper to paper. In this work, the definition for V is given in equation (1) while we will use several forms for the photon count N . With no subscript, N will denote the expected number of photon events in a single pixel during one sample. Adding subscripts to N will denote the sum over subsets of pixels. Thus N_ν is the expected number of counts summed across all the spectral pixels within a single fringe phase channel, while N_Φ denotes the expected number of counts summed across all the fringe phase pixels within a single spectral channel. The expected number of detected photon events across all pixels is written $N_{\nu\Phi}$. Since the spectral pixels are arranged evenly in wavenumber space they will not necessarily contain the same average counts per cycle, however, a good approximation is that

$$N_{\nu\Phi} = P_\Phi \times N_\nu = P_\nu \times N_\Phi. \quad (9)$$

When working through the SNR calculations, it is easiest to use the expected number of photon events in a single pixel N . However, when comparing these expressions it is best to use the number of events in an entire spectral channel N_Φ .

The angular brackets in equation (8) denote an ensemble average, that is, if one could freeze the atmosphere and the OPD at their positions at time $k\tau$ and make multiple measurements we would find that c_{ijk} would follow Poisson statistics with an expected value given by equation (8). In the calculations to follow a second type of average will be used, denoted by a line above a variable, indicating an average across many samples while the atmosphere is free to move. The noise term r_{ijk} will be modeled as a Gaussian process with zero mean and a standard deviation of σ . In the case of a CCD, σ corresponds directly to the readout noise. These and other statistics issues are addressed in more detail in Appendix A.

3 Correlation measurement

The primary goal of an interferometer is to measure $|\gamma(\nu_j)|$, the visibility magnitude at a given wavelength at the current projected baseline. In order to do this, we measure the apparent visibility $V(\nu_j)$ and calibrate for the coherence transfer factor $\eta(\nu_j)$ by switching between an unresolved, or well known, object and the object of scientific interest. There are many methods for measuring V , almost all of which result in an estimate for V^2 , called the correlation. Each method, however, has a slightly different form for the SNR. In this paper,

we will consider three methods in detail: A direct DFT, an example of the DFT method first proposed by Tango and Twiss[5], and a modified version of the Tango and Twiss method.

In the analysis that follows, we will consider two cases: one in which the detector noise is well known in advance of the correlation measurement, which we shall refer to as the “known-noise” case, and one in which we are estimating σ with the same data as that used to estimate the correlation $V(\nu_j)$ which we shall refer to as the “unknown-noise” case. In general, the known-noise case produces a better SNR than does the unknown-noise case, however the former relies on knowing the noise properties of the detector in advance, something that will not always be the case. Since a correlation measurement is made independently in each spectral channel, in many places the j subscripts will be removed for the sake of notational clarity.

3.1 Discrete Fourier Transform

If the fringe phase dimension of the detector has at least 4 pixels, one can use a DFT to estimate the visibility. In most practical systems, the fast Fourier Transform (FFT) is used but this does not affect the results. In the case of the frequency bin that corresponds to the spatial frequency of the fringes, $s = s_\Phi(\nu_j)$ and the total power is the signal power $N_\Phi^2 V^2/4$ plus the noise power. The noise power is the sum of the variances of the two sources of noise, photon statistics and detector noise. The variance of the photon events is N_Φ while the variance of the detector noise will be $P_\Phi \sigma^2$. Frequency bins that do not correspond to the fringe spatial frequency will contain only noise power. This means that the power spectrum averaged over many samples will have the form

$$\overline{|\Lambda_\Phi(s)|^2} = \begin{cases} N_\Phi^2 + N_\Phi + P_\Phi \sigma^2 & \text{for } s = 0 \\ N_\Phi^2 V^2/4 + N_\Phi + P_\Phi \sigma^2 & \text{for } s = s_\Phi(\nu_j) \\ N_\Phi + P_\Phi \sigma^2 & \text{otherwise.} \end{cases} \quad (10)$$

Once the noise power $N_\Phi + P_\Phi \sigma^2$ is subtracted, the signal in the $s = s_\Phi(\nu_j)$ bin is a correlation measurement. The SNR of this measurement of fringe visibility for the “known-noise” case, not including double frequency or other terms assumed insignificant, is given by Beletic[10] as

$$\text{SNR}(V^2) = \frac{\sqrt{M} N_\Phi^2 |T(\nu_j)|^2 |\gamma(\nu_j)|^2}{\sqrt{N_\Phi^2 + 2N_\Phi^3 |T(\nu_j)|^2 |\gamma(\nu_j)|^2 + 2P_\Phi \sigma^2 (N_\Phi^2 |T(\nu_j)|^2 |\gamma(\nu_j)|^2 + N_\Phi) + P_\Phi^2 \sigma^4}} \quad (11)$$

where $T(\nu_j)$ is the normalised optical system transfer function. In order to measure V^2 with the DFT, we need to set $|T(\nu_j)| = \eta/2$ and $|\gamma(\nu_j)| = V$ yielding

$$\text{SNR}(V^2) = \frac{\sqrt{M} N_\Phi^2 V^2}{4\sqrt{N_\Phi^2 + \frac{1}{2}N_\Phi^3 V^2 + 2P_\Phi \sigma^2 (\frac{1}{4}N_\Phi^2 V^2 + N_\Phi) + P_\Phi^2 \sigma^4}}. \quad (12)$$

In the high photon count limit ($N \gg 1$) this expression can be approximated by $\frac{1}{2}\sqrt{\frac{MN}{2}}V$ for both a noiseless and a noisy detector. For a noiseless detector at low light levels ($N \ll 4/V^2$)

$$\text{SNR}_{\text{noiseless}}(V^2) \approx \frac{\sqrt{M}V^2N_{\Phi}}{4} \quad (13)$$

while for a known-noise detector

$$\text{SNR}_{\text{noisy}}(V^2) \approx \frac{\sqrt{M}N_{\Phi}^2V^2}{4P_{\Phi}\sigma^2}. \quad (14)$$

3.2 The Tango and Twiss Method

Clearly, the SNR is a strong function of the number of pixels and so we will investigate in more detail a DFT method that uses the minimum number of 4 pixels. This involves a single pixel detector on either side of the beam splitter while inserting a quarter-wave plate into one beam every other cycle, which is equivalent to setting $P_{\Phi} = 4$ and $s_{\Phi}(\nu_j) = 1$. The measurement technique used on the Mark III interferometer[15] involves integrating over the fringes in four fringe phase bins using a temporal modulation of the optical path length but is essentially the same.

We form the biased and unnormalised fringe correlation estimate for the k th sample in the j th spectral channel

$$q_k = (n_{1k} - n_{3k})^2 + (n_{2k} - n_{4k})^2 \quad (15)$$

with the expectation value over many samples of

$$\overline{\langle q \rangle} = 4N^2V^2 + 4N + 4\sigma^2. \quad (16)$$

This represents a measurement of the signal power plus the noise power. We can estimate the photon noise power by summing the counts in all four fringe phase pixels, and we find that

$$\overline{\langle \sum_{i=1}^4 n_i \rangle} = 4N \quad (17)$$

which can be subtracted from our biased estimator $\overline{\langle q_j \rangle}$ to remove the effects of photon noise. The detector noise term $4\sigma^2$, however, still needs to be removed. If we know the detector's noise characteristics in advance, this can be done easily. We thus arrive at the "known-noise" estimator for fringe correlation

$$\overline{\langle C_N^2 \rangle} = \frac{\overline{\langle q \rangle} - \overline{\langle \sum_{i=1}^4 n_i \rangle} - 4\sigma^2}{4N^2} \quad (18)$$

whose value will converge to V^2 .

The SNR of this estimate (derived in detail in Appendix A) is

$$\text{SNR}(V^2) = \frac{\sqrt{M}N_{\Phi}^2V^2}{4\sqrt{N_{\Phi}^2 + \frac{1}{2}N_{\Phi}^3V^2 + 8\sigma^2(\frac{1}{4}N_{\Phi}^2V^2 + N_{\Phi} + \frac{1}{2}) + 16\sigma^4}}. \quad (19)$$

Note that, apart from the factor of $1/2$ (a term assumed insignificant by Beletic), this is identical to equation (12) with $P_\Phi = 4$.

If the detector noise properties are not well known in advance we need to estimate the noise at the same time as estimating the signal correlation. This can be done by simultaneously calculating

$$\overline{\langle (\sum_{i=1}^4 n_i)^2 \rangle} = 16N^2 + 4N + 4\sigma^2 \quad (20)$$

and forming the “unknown-noise” fringe correlation estimator

$$\overline{\langle C_N^2 \rangle} = \frac{\overline{\langle q \rangle} - \overline{\langle (\sum_{i=1}^4 n_i)^2 \rangle}}{4N^2} + 4. \quad (21)$$

with the SNR

$$\text{SNR}(V^2) = \frac{\sqrt{MN_\Phi^2 V^2}}{4\sqrt{\frac{1}{4}N_\Phi^3(16 - 6V^2) + N_\Phi^2(4 - V^2) + \sigma^2[N_\Phi^2(16 + 2V^2) + 24N_\Phi] + 64\sigma^4}}. \quad (22)$$

An inspection of equations (19) and (22) makes it clear that the known-noise estimator will always have a better SNR than the unknown-noise estimator. However, it is likely that the unknown-noise estimator will produce more reliable results in the long term as the noise characteristics of the detector evolve with time and environmental conditions.

The high light level limit is independent of the detector noise and for the known-noise case is

$$\text{SNR}(V^2) \approx \frac{1}{2}\sqrt{\frac{MN_\Phi}{2}}V. \quad (23)$$

Note that the high light level limit will not be the same for the unknown-noise case. This is because there will always be extra noise added when estimating the detector noise, resulting in a lower SNR for all flux levels. For low light levels, there are different approximations for the noiseless and noisy cases. For a noiseless detector

$$\text{SNR}_{\text{noiseless}}(V^2) \approx \frac{\sqrt{MV^2 N_\Phi}}{4} \quad (24)$$

while for a noisy detector

$$\text{SNR}_{\text{noisy}}(V^2) \approx \frac{\sqrt{MN_\Phi^2 V^2}}{\mathcal{X}\sigma^2} \quad (25)$$

where $\mathcal{X} = 16$ for the known-noise case and $\mathcal{X} = 32$ for the unknown-noise case.

3.3 Modified Tango and Twiss Method

The Tango and Twiss method produces a correlation estimate for every sample and can also be used to supply an estimate for the fringe phase every cycle. If we forgo these features, it

is possible to produce a correlation estimator that uses only two pixels and thereby achieve a better SNR which we shall call the “modified Tango and Twiss method”. For this method to work, we must assume that the atmosphere changes the fringe phase randomly and the cosine terms average out according to equation (54). This was the method used in the Sydney University Stellar Interferometer (SUSI) prototype and, at the time of writing, the SUSI[16] instrument itself. In this measurement scheme, $P_\Phi = 2$ and, as before, $s_\Phi(\nu_j) = 1$, which is equivalent to a single pixel per spectral channel on either side of a beam splitter. The biased and unnormalised estimator then becomes

$$q_k = (n_{1k} - n_{2k})^2 \quad (26)$$

which has the expectation over many samples of

$$\langle q \rangle = 2N^2V^2 + 2N + 2\sigma^2. \quad (27)$$

Once again we must subtract out the noise power terms $2N$ and $2\sigma^2$. The known-noise and unknown-noise cases are similar to the Tango and Twiss method described above. In the known-noise case we use

$$\langle C_N^2 \rangle = \frac{\langle q \rangle - \overline{\langle \sum_{i=1}^4 n_i \rangle} - 2\sigma^2}{2N^2}. \quad (28)$$

This has a SNR of

$$\text{SNR}(V^2) = \frac{\sqrt{M}N_\Phi^2V^2}{4\sqrt{\frac{1}{32}N_\Phi^4V^4 + \frac{1}{2}N_\Phi^3V^2 + \frac{1}{2}N_\Phi^2 + \sigma^2(N_\Phi^2V^2 + 2N_\Phi + \frac{1}{2}) + 2\sigma^4}}. \quad (29)$$

The unknown-noise estimator is

$$\langle C_N^2 \rangle = \frac{\langle q \rangle - \overline{\langle (\sum_{i=1}^4 n_i)^2 \rangle}}{2N^2} + 2 \quad (30)$$

which has a SNR of

$$\text{SNR}(V^2) = \frac{\sqrt{M}N_\Phi^2V^2}{4\sqrt{\frac{1}{32}N_\Phi^4V^4 + (N_\Phi^3 + N_\Phi^2)(1 - \frac{1}{2}V^2) + 2\sigma^2[N_\Phi^2(1 + \frac{1}{2}V^2) + 2N_\Phi] + 4\sigma^4}}. \quad (31)$$

In contrast to the other correlation estimators, while the SNR in a single sample will always increase with increasing photon events, it has a maximum asymptotic value of

$$\lim_{N \rightarrow \infty} \text{SNR}(V^2) = \sqrt{2M} \quad (32)$$

for both equation (29) and equation (31). This is because this measurement method relies on an average over many samples to obtain a correlation estimate, whereas the DFT methods yield a correlation measurement for each sample. In the modified Tango and Twiss method

a single sample is not a good estimator for signal correlation and can never have an SNR greater than $\sqrt{2}$.

For the low photon count levels we have for a noiseless detector

$$\text{SNR}_{\text{noiseless}}(V^2) \approx \frac{1}{2} \sqrt{\frac{M}{2}} N_{\Phi} V^2, \quad (33)$$

while for a noisy detector

$$\text{SNR}_{\text{noisy}}(V^2) \approx \frac{\sqrt{M} N_{\Phi}^2 V^2}{\mathcal{X} \sigma^2} \quad (34)$$

where $\mathcal{X} = 4\sqrt{2}$ in the known-noise case and $\mathcal{X} = 16$ for the unknown-noise case.

3.4 Comparison

It is clear from the above analysis that the SNR is a strong function of pixel number for a noisy detector. Thus, when measuring signal correlation it is most advantageous to pick the measurement scheme that uses the least number of pixels. We will therefore restrict ourselves to the Tango Twiss method, a four pixel DFT, and the modified Tango and Twiss method.

Figure 2 contains a number of plots of the predicted SNR in a single sample as a function of detected photon events for various visibilities and detector noise values. The value of $\sigma = 6$ has been chosen as a value for production CCD detector arrays. We will also use a value of $\sigma = 3$ in some calculations representing a ‘current best’ value for CCDs. As one would expect, a noiseless detector system achieves the best SNR for any given photon count. These plots also show that the modified Tango and Twiss measurement scheme performs the best at low count rates, while it goes to $\sqrt{2M}$ for high count rates as per equation (32). This holds true for both the known-noise and unknown-noise cases. For correlation measurements then, the modified Tango and Twiss estimator is preferable whether one is using a noisy detector or not.

In order to compare the noisy case with the noiseless case we must also take into account the DQE of the different types of detector. Figure 3 contains plots of predicted SNR and predicted integration times for the noiseless and the known-noise modified Tango and Twiss estimator where in the case of the noiseless detector the DQE has been set to 10% and for the noisy detector the DQE has been set to 80%. The 10% figure is higher than any currently available photon noise limited array detector while the 80% figure is slightly lower than the best DQE’s reported for a CCD. The topmost plot in figure 3 shows the predicted SNR for visibilities of 1 and 0.25. At the lowest count rates, the noiseless detector has the best performance. This will always be true even if the noisy detector were 100% efficient. However, the noisy detector has a better SNR for a substantial range of count rates. The crossover point occurs at $N_{\Phi} \approx 3$ when $\sigma = 3$ and at $N_{\Phi} \approx 10$ when $\sigma = 6$ for both visibilities.

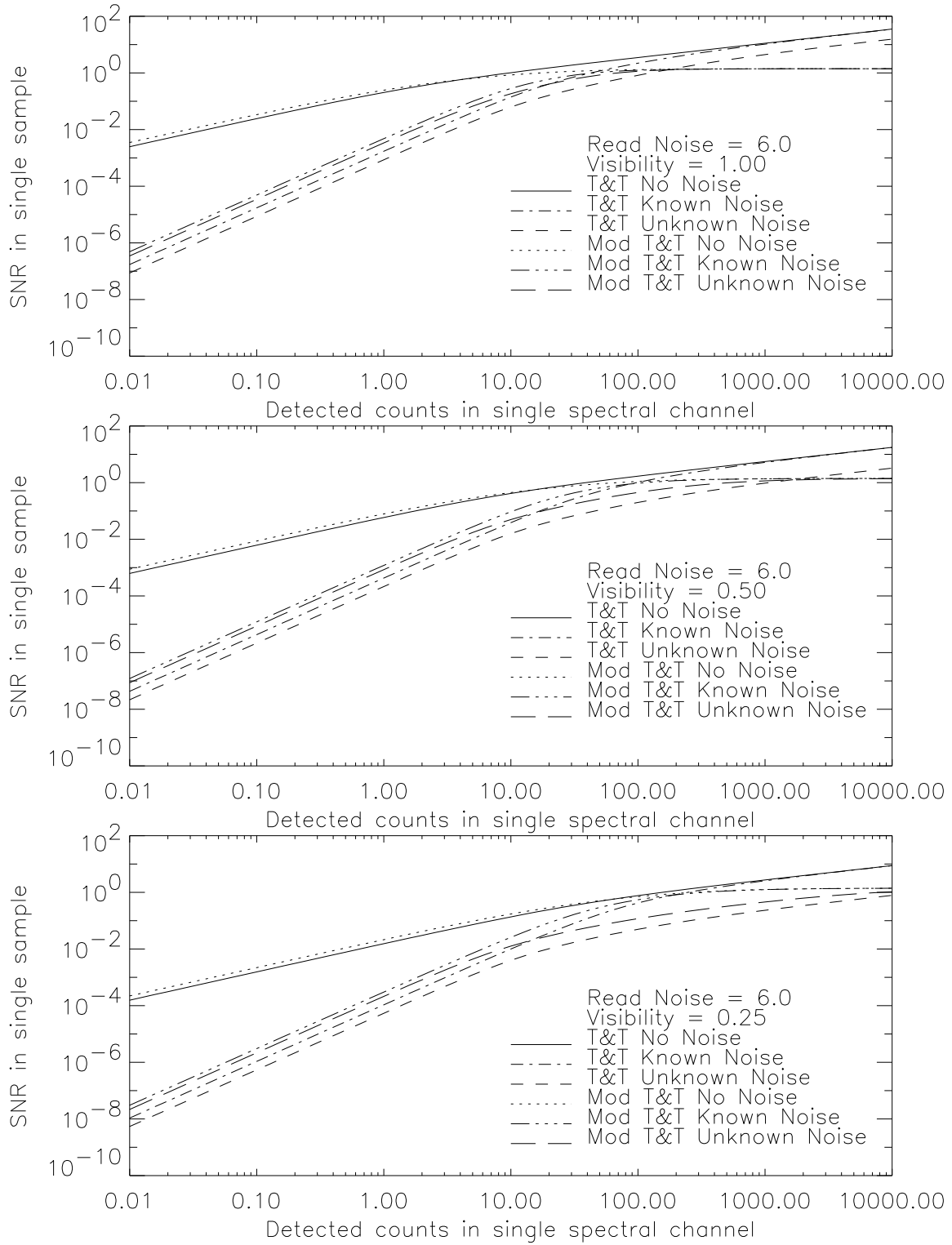


Figure 2: Plots of SNR for the Tango/Twiss and Modified Tango/Twiss measurement methods for a range of visibilities and a noise value of 6.

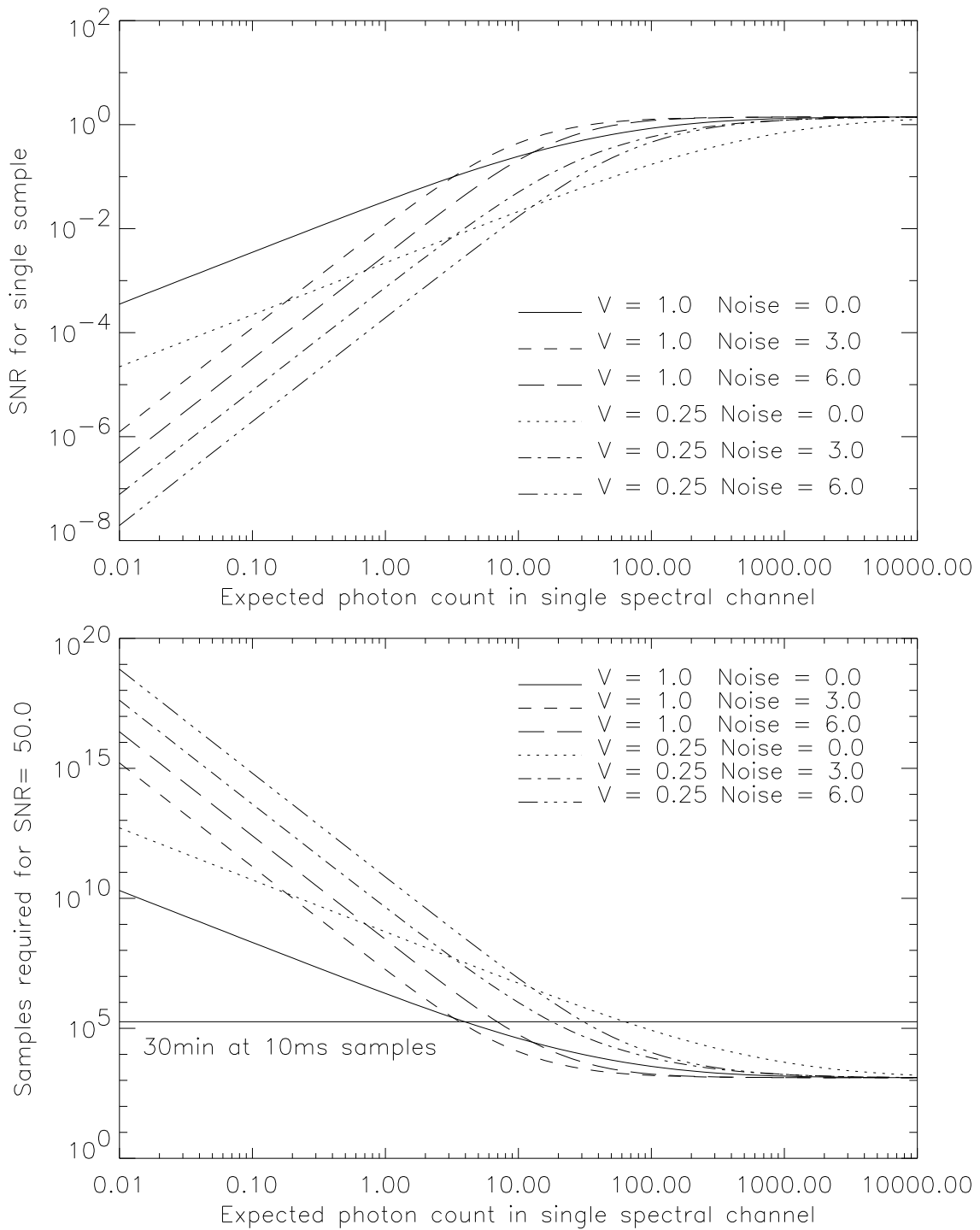


Figure 3: Comparison of a noiseless and noisy detector using the known-noise modified Tango and Twiss method. The top plot shows the expected SNR while the bottom plot shows the number of samples required for a total SNR of 50. The noiseless detector is assumed to have a DQE of 10% while the noisy detector has a DQE of 80%.

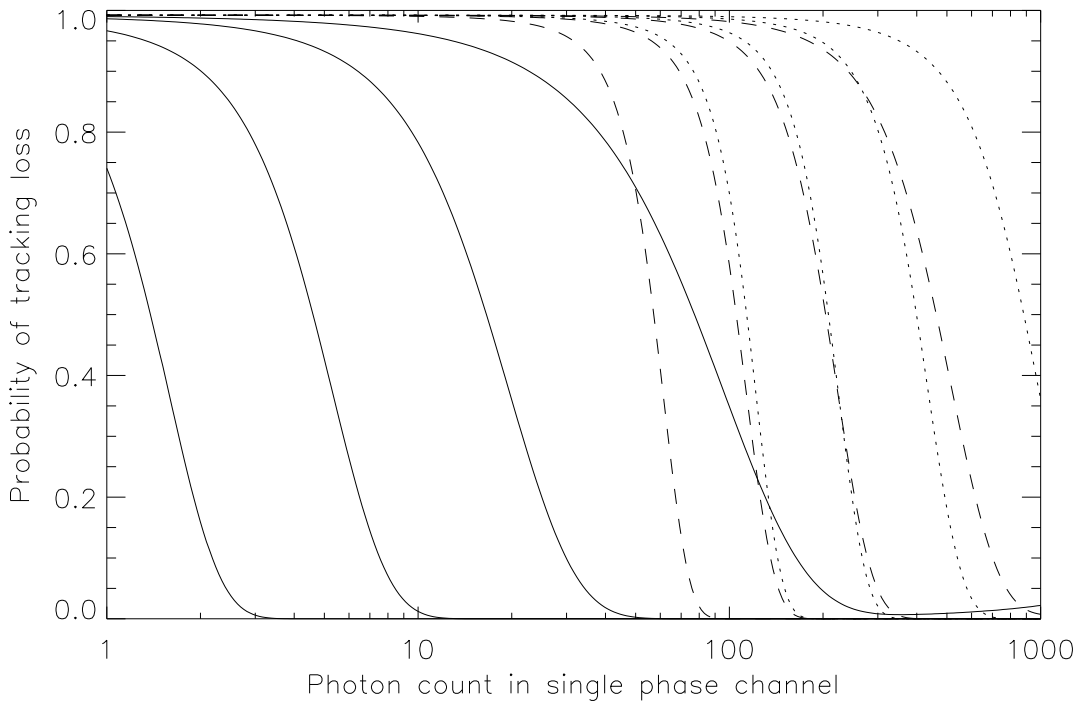


Figure 4: The probability of tracking failure for a visibility of 0.5 measured across 256 pixels and setting $b = 127$ (all DFT pixels except the DC channel) with no noise (solid lines), a noise of $\sigma = 3$ (dashed lines) and noise of $\sigma = 6$ (dotted lines). Four integration times are shown for each noise level which are from right to left: $M = 1$, $M = 10$, $M = 100$ and $M = 1000$.

Another way of comparing the detectors is shown in the lower plot of figure 3. This plot contains the same data except the vertical axis now represents the number of samples required in an integration to achieve a SNR of 50. An horizontal line has also been added representing an half-hour integration for a sample time of 10ms. In the case of a visibility of 1, it is only at this point that the noiseless detector starts to be a better choice than the noisy detector, for both the $\sigma = 3$ and the $\sigma = 6$ cases. For lower visibilities, this does not occur until integrations several orders of magnitude longer are used, by which time the projected baseline will have changed significantly. The measured visibility will always be less than one. Thus in terms of required integration times for a given SNR, a noisy detector may be quite adequate for correlation measurement. For example, for an aperture size of 20cm, the sample time of 10ms quoted above, an optical system throughput of 5% and an optical bandwidth of 3nm a noisy detector will have magnitude limit of 8 in the case of $V = 1$ after an half-hour integration, the same as that of the noiseless detector. For the $V = 0.25$ case, the magnitude limits are 6 for $\sigma = 3$, 5.5 for $\sigma = 6$ and 4.7 for the noiseless detector. While using a high-DQE single-pixel photon noise limited detector, like APDs, would achieve better magnitude limits, if one already has an array detector available (like a CCD) the latter could be used for correlation measurement.

4 Group delay tracking

The fringe envelope must be located and tracked before any correlation measurements can be made, and, unless some form of passive interferometry is used, the fringe tracking system will define the magnitude limit of the instrument. Fringe tracking can take two forms; phase locking where the tracking servo loop is closed to within a fraction of the fringe phase, or group delay tracking (GDT) which is less precise and tracks to within a fraction of the fringe envelope. In this analysis we shall use GDT for several reasons. To begin with, phase locking requires at least four pixels in the fringe phase dimension of the detector, either by using a temporal encoding scheme like that used in the Mark III or with wave-plates as in the Tango and Twiss method. This means phase tracking is wavelength dependent, requires many pixels, and, given the same DQE, will have a brighter magnitude limit than GDT. In contrast, GDT requires only a single fringe phase pixel in each spectral channel. Secondly, when phase locking fails, it does so catastrophically while even once GDT has failed for actively tracking the fringe envelope, it can be used for passive tracking and post-processing. Finally, in order for some of the correlation measurement schemes to work, we have assumed that a residual phase error occurs due to the atmosphere. This will not be true for phase locking.

Group delay tracking relies on the fact that the spatial frequency of the fringes in the spectral dimension of the detector is linearly related to the OPD. In order to find the current OPD we calculate a DFT across the spectrum which gives us

$$\overline{|\Lambda_\nu(s)|^2} = \begin{cases} N_\nu^2 + N_\nu + P_\nu\sigma^2 & \text{for } s = 0 \\ N_\nu^2 V^2/4 + N_\nu + P_\nu\sigma^2 & \text{for } s = s_\nu \\ N_\nu + P_\nu\sigma^2 & \text{otherwise,} \end{cases} \quad (35)$$

and search for a peak. The frequency bin containing this peak should be that corresponding to $s = s_\nu$, and equation (4) can then be used to find the OPD. This will fail to give the correct result if the noise causes the highest peak to be in a frequency bin other than $s = s_\nu$. Thus the SNR of the DFT estimator is not as important in fringe tracking as the probability that some noise peak will be higher than the signal peak. In this analysis we shall follow the work by Lawson[9] in which a complete description of the GDT method using a photon noise limited detector can be found.

In order to calculate the probability of tracking failure, we need the Rayleigh and Rician probability density functions, first used in interferometry by Walkup and Goodman[17]. These distributions represent, respectively, the noise probability density function and the signal plus noise probability density function of the DFT of the fringe signal. The probability that the energy in a given channel of the Fourier transform lies between Z and $Z + dZ$ is given by

$$P(Z, s) = \frac{Z}{\sigma_Z^2} \exp \left[-\frac{1}{2\sigma_Z^2} (Z^2 + |\Lambda(s)|^2) \right] I_0 \left(\frac{|\Lambda(s)|Z}{\sigma_Z^2} \right) \quad (36)$$

where $I_0(x)$ is the modified Bessel function of order zero. The second moment of the distri-

bution is

$$\langle Z^2 \rangle = |\Lambda(s)|^2 + 2\sigma_Z^2. \quad (37)$$

Due to the similarities of equation (35) to equation (37), we set $|\Lambda(s)| = \frac{N_\nu V}{2}$ for the Rician distribution, $|\Lambda(s)| = 0$ for the Rayleigh distribution, and in both cases $2\sigma_Z^2 = N_\nu + P_\nu \sigma^2$.

If one were to average the power spectra over M samples the probability density distributions will no longer be simple Rician or Rayleigh distributions. Instead they will be these distributions convolved with themselves M times. Methods for calculating these probability density functions for single and multiple samples are detailed by Lawson[9].

The probability that at least one noise peak amongst b channels is higher than the signal peak is given by[9]

$$p_e = 1 - \int_0^\infty P(Z, s = s_\nu) \left[\int_0^Z P(Z, s \neq s_\nu) dz \right]^b dZ \quad (38)$$

where $P(Z, s = s_\nu)$ is the probability density function of the signal plus the noise and $P(Z, s \neq s_\nu)$ is the probability density function of the noise only. Equation (38) represents the probability of tracking failure, that is, the probability that a noise spike will be mistaken for the fringe signal. An important consideration when performing this calculation is the choice of a value for b . If the fringe location is totally unknown, the value of b must be set to the number of frequency bins in the DFT. If it is known that the fringes could not have moved more than a small distance since the last measurement, the value of b can be reduced.

Several examples of tracking loss probability curves are shown in figure 4 for channeled spectra with $P_\nu = 256$ and a measured visibility of 0.5. The search for a peak is across all pixels in the DFT excluding the zero frequency or DC channel, and so $b = 127$. The calculations have been performed for three levels of noise: $\sigma = 0$, $\sigma = 3$ and $\sigma = 6$; and for integrations across 1, 10, 100 and 1000 samples. In each case, the DQE of the detector has been set to 100%. The addition of detector noise has two effects. The first, and most detrimental, is to increase the number of detected photon events required to maintain tracking. The second effect is an increased slope in the probability of tracking loss with reduced photon counts. This second effect is similar to changing the b parameter.

As with the comparison of correlation measurements in section 3.4, a more practical way to judge the effect of detector noise is to take into account the difference in DQE of the two types of detector. Several sets of probability curves have been plotted in figure 5 for a range of integration times and visibility values of 0.25, 0.5 and 1.0. Once again the DQE of the noiseless detector has been set to 10% and that of the noisy detector to 80% with a noise level of $\sigma = 3$. These represent best cases for an intensified CCD or photon counting array using an image intensifier and a modern bare CCD. For the highest visibility levels and longest integration times, the noiseless detector still has the best performance. However, unresolved objects will never be the major target of a stellar interferometer. At the lower visibilities and shorter integration times the noisy detector starts to out-perform the noiseless detector, with the only disadvantage being the increased slope of the curve implying that failure will

be more catastrophic. If we take into account the other features of a CCD, relatively low cost, flexibility due to noiseless on-chip rebinning and large optical bandwidth, the CCD becomes an attractive device for use in group delay tracking. Furthermore, if the number of pixels P_ν is reduced, the effect of detector noise is reduced, making a high-DQE, noisy detector even more promising.

As an illustration of the potential of a noisy detector, consider tracking an object whose measured visibility at the current baseline and atmospheric conditions is 0.5. Using the same sample time of 10ms, aperture size of 20cm and optical throughput of 5% used in section 3.4 and the optical configuration shown in figure 1, it is possible to estimate the magnitude limit of fringe tracking. Since there is a spectrum available on both sides of the beam splitter, two channeled fringes are available and the probability of tracking loss may be squared reflecting the likelihood that both channels lose the fringe signal. Table 1 contains the magnitudes at which the probability of tracking loss is 1%, once again using the 10% and 80% DQE figures for the noiseless and noisy detectors and setting $P_\nu = 64$ and $b = 31$. The noisy detector has a higher magnitude limit in all cases. As the integration M is increased the effects of detector noise increases, reflecting the fact that many ‘readouts’ of the detector are required. At high values of M , the noiseless detector starts to out-perform the noisy detector. However, for active fringe tracking, a detector capable of tracking in the shortest possible integration time is desired. Clearly a noisy detector such as a CCD is suitable for group delay tracking and, if a large aperture were broken up into multiple subapertures, even fainter objects could be targeted.

4.1 Gaussian approximation

The numerical calculation of the integrals in equation (38) are time consuming. Because one is typically more interested in the point at which the probability is significantly greater than zero, and not the exact probability for all light levels, it is useful to have an approximate form for the point of tracking failure. In the limit of large values of M , both the Rician and Rayleigh distributions when convolved with themselves M times are well approximated by a Gaussian. Thus we can approximate equation (38) by using Gaussian probability density functions over $Z(s)$ with a mean of

$$\overline{Z(s)} = |\Lambda(s)|^2, \quad (39)$$

where for the signal plus noise distribution we set $|\Lambda(s = s_\nu)| = NV/2$ and for the noise only distribution $|\Lambda(s \neq s_\nu)| = 0$. Following equation (12), we set the variance of both the signal plus noise distribution and the noise only distribution to

$$\sigma_{Z(s)}^2 = \frac{1}{M} [N_\nu^2 + 2N_\nu|\Lambda|^2 + 2P_\nu\sigma^2(|\Lambda|^2 + N_\nu) + P_\nu^2\sigma^4]. \quad (40)$$

Rather than calculate equation (38) fully, we note that, as shown by Lawson[9], this integral is really a calculation of the overlap of the two probability distributions. A large

Table 1: Fringe tracking magnitude limits for noiseless and noisy detectors.

M	DQE = 10%	DQE = 80%	
	$\sigma = 0$	$\sigma = 3$	$\sigma = 6$
1	6.6	7.8	7.2
10	8.4	8.9	8.2

overlap corresponds to a high probability of tracking loss while a small overlap implies a low probability of tracking loss. Thus, using the Gaussian approximation above, we can say that tracking failure will occur when the difference in means is less than the sum of the $\beta\sigma_{Z(s)}$ points for the two distributions. This will be when

$$\overline{Z(s = s_\nu)} - \overline{Z(s \neq s_\nu)} = \beta [\sigma_{Z(s=s_\nu)} + \sigma_{Z(s \neq s_\nu)}] \quad (41)$$

where in most cases we shall set $\beta = 3$. If we combine equations (39), (40) and (41) we find that the visibility at which tracking will fail is

$$V^2 = \frac{8\beta}{MN_\nu^2} \left(N_\nu + P_\nu\sigma^2 + \frac{1}{\beta} \sqrt{M(N_\nu^2 + P_\nu^2\sigma^4 + 2P_\nu\sigma^2N_\nu)} \right). \quad (42)$$

This equation can also be solved numerically for N_ν . This has been done for the various parameters sets shown in figure 5 where small vertical lines have been plotted at the photon count rate predicted by equation (42). This plot demonstrates that the Gaussian approximation works well, even for low values of M .

5 Sample time and aperture size optimisation

With the approximations for correlation measurement SNR set out in section 3 and the Gaussian approximation given in the previous section for tracking failure, it is possible to investigate optimum sample times and aperture sizes for the two measurements. In order to do this we require expressions for the temporal and spatial correlation transfer factors of the atmosphere. The temporal coherence transfer factor is given by[6]

$$\eta_t^2 = \frac{2}{\tau} \int_0^\tau \left(1 - \frac{t}{\tau}\right) \exp \left[-\left(\frac{t}{\tau_0}\right)^{5/3} \right] dt, \quad (43)$$

and the spatial coherence transfer factor is given by[5]

$$\eta_s^2 = \frac{\int T(\boldsymbol{\nu})B^2(\boldsymbol{\nu}) d\boldsymbol{\nu}}{\int T(\boldsymbol{\nu}) d\boldsymbol{\nu}}. \quad (44)$$

Once again $T(\boldsymbol{\nu})$ is the optical transfer function of the optical system, and the optical transfer function of the phase aberrations caused by the atmosphere is $B(\boldsymbol{\nu})$. Expressions for $T(\boldsymbol{\nu})$ and $B(\boldsymbol{\nu})$ can be found in the work by Fried[18].

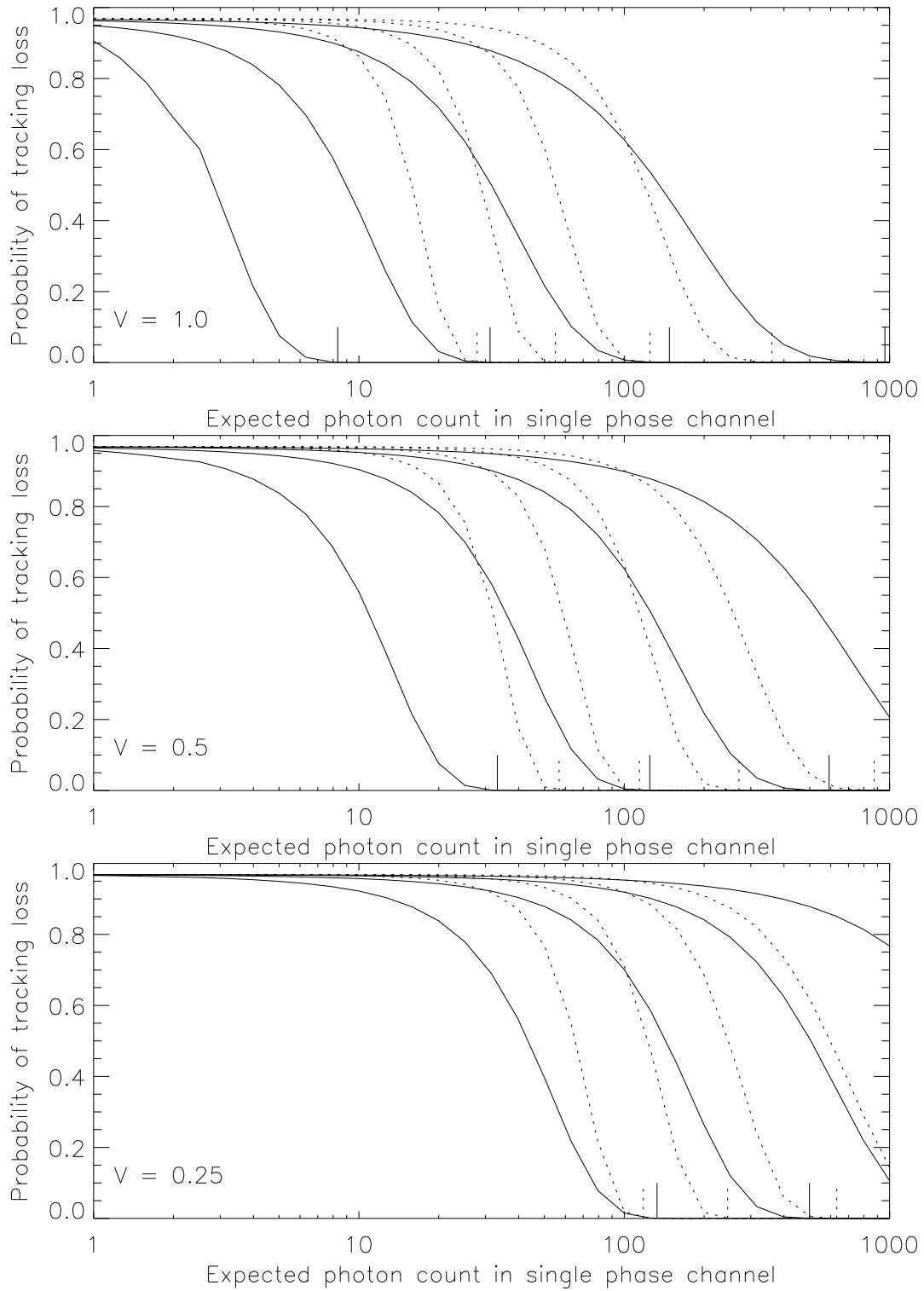


Figure 5: Probability of tracking loss for a range of visibilities. The solid lines represent a 10% noiseless detector while the dashed lines represent an 80% detector with $\sigma = 3$. From right to left, the plots are for $M = 1$, $M = 10$, $M = 100$ and $M = 1000$. The short vertical lines along the horizontal axis are the approximated tracking failure points.

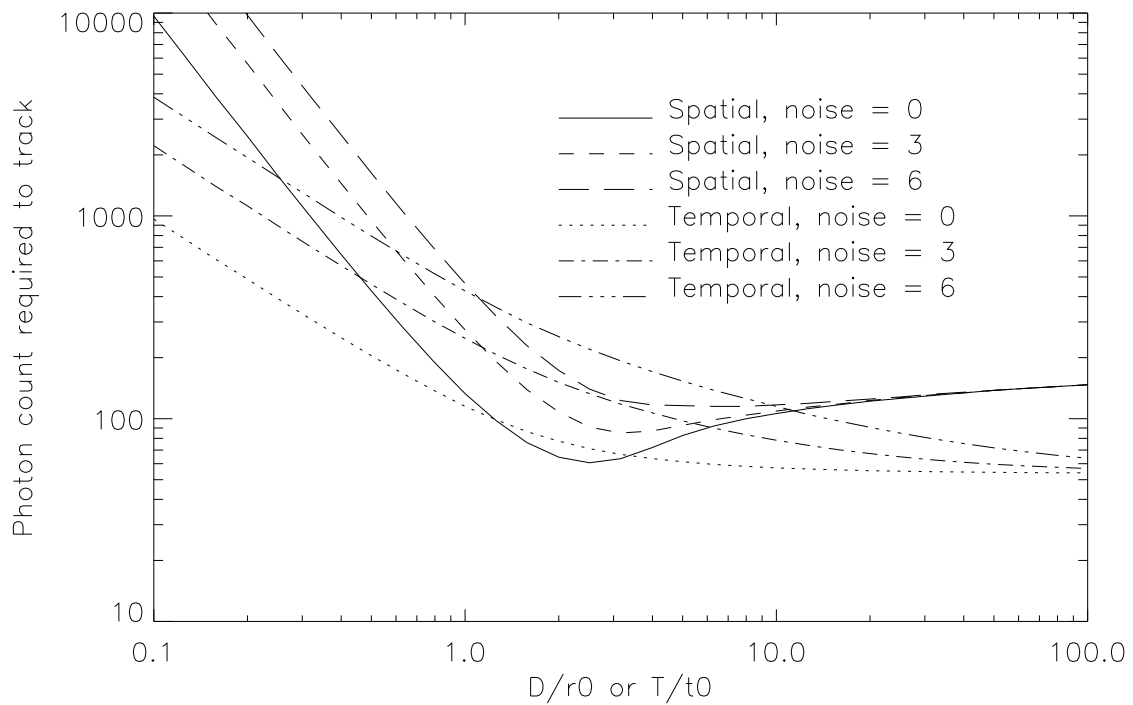
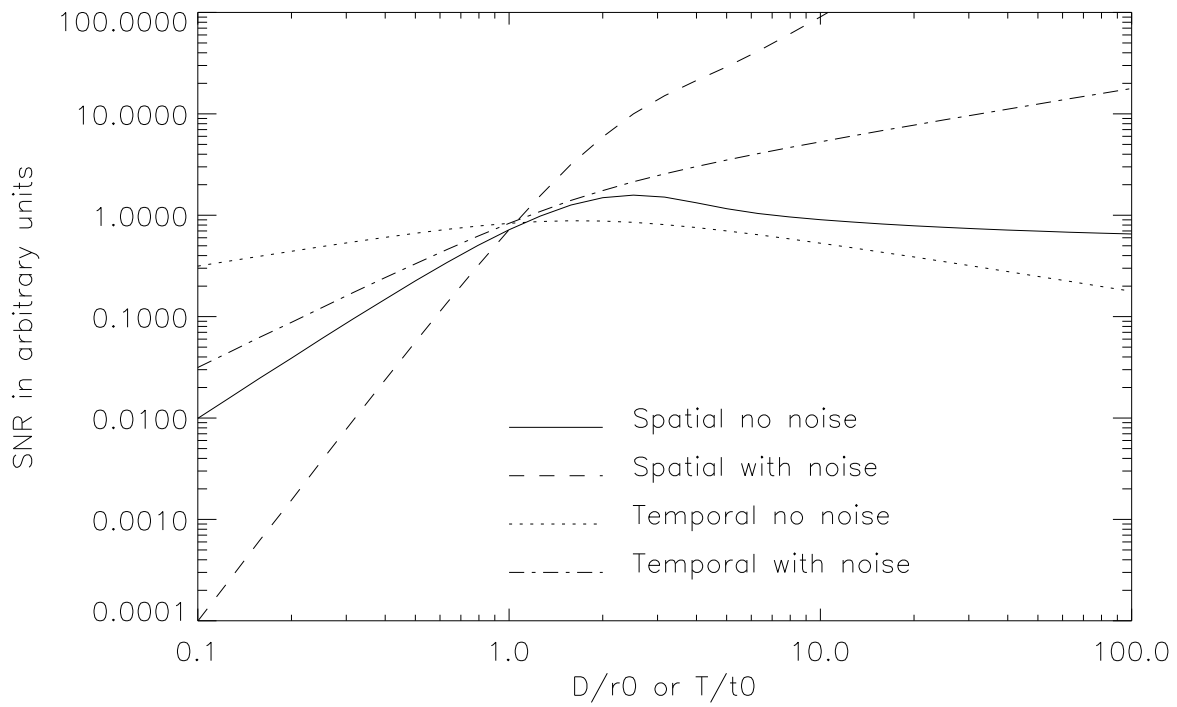


Figure 6: Above: The SNR of correlation measurement at low photon rates in arbitrary units. The four lines plotted are for a variation in: the aperture size for a noiseless (solid line) and a noisy detector(dashed line); the sample time for a noiseless (dotted line) and a noisy detector (dash-dot line). Below: A similar plot showing the photon counts required to track the fringe envelope in a single sample over each r_0 cell, using a 32 pixel detector. Again lines are plotted for both a change in aperture size and a change in sample time for various levels of detector noise.

5.1 Correlation measurement

For correlation measurement we have, for all measurement schemes,

$$\text{SNR}(V^2) \propto \begin{cases} \sqrt{M} N_{\Phi} V^2 & \text{for } \sigma = 0 \\ \sqrt{M} N_{\Phi}^2 V^2 & \text{for } \sigma \neq 0. \end{cases} \quad (45)$$

Changing the sample time will affect all of the parameters in equation (45). The visibility V will be proportional to the temporal coherence transfer factor given in equation (43), the average number of photons arriving per sample time will be proportional to the sample time while the number of samples M in a given integration time will be inversely proportional to the sample time. This results in

$$\text{SNR}(V^2) \propto \begin{cases} \tau^{1/2} \eta_t^2 & \text{for } \sigma = 0 \\ \tau^{3/2} \eta_t^2 & \text{for } \sigma \neq 0. \end{cases} \quad (46)$$

Changing the aperture size R will have a similar effect, except the number of integrations will not change and the average number of photons will be proportional to the aperture radius squared, and so

$$\text{SNR}(V^2) \propto \begin{cases} R^2 \eta_s^2 & \text{for } \sigma = 0 \\ R^4 \eta_s^2 & \text{for } \sigma \neq 0. \end{cases} \quad (47)$$

The top plot in figure (6) shows the SNR in arbitrary units for the these four cases.

From the point of view of SNR a noiseless detector has an optimum sample time of $1.6\tau_0$ and an optimum aperture size of $2.5r_0$. Taking into account the different definitions of η_s , this is exactly the same as the results of Buscher. Once detector noise has been added, however, no local maximum occurs in the SNR curves and both the optimum aperture size and sample time go to infinity. This is similar to the non tilt corrected case discussed by Buscher. Obviously it is neither possible nor desirable to have extremely large sample times or apertures which will produce very low measured visibilities, albeit with high SNR. As will be shown below, this is not the case for group delay tracking, and when using the same detection system to do both fringe tracking and correlation measurement it would be best to choose the aperture size that optimises fringe tracking performance. Figure 6 also shows that the curves for the noisy detector change slope at approximately the same point at which the noiseless detector SNR is optimised. This indicates that while the SNR will increase beyond this point, the relative increase in SNR is reduced. Thus using the optimum sample time for a noiseless detector may be the best choice even if you are using a noisy detector.

5.2 Fringe tracking

Unfortunately, no simple approximations are available for group delay tracking, so no general case can be investigated. The lower plot in Figure 6 shows the count rates required per r_0 cell in a time period of τ_0 for group delay tracking using equation (42) over 32 pixels with

noise levels of $\sigma = 0$, $\sigma = 3$ and $\sigma = 6$ and no integration ($M = 1$). Once again, equations (43) and (44) have been used for the visibility, and the counts have been scaled by R^2 for the spatial case and τ for the temporal case.

For a noiseless detector, the optimum aperture size is once again $2.5r_0$, the same as that for correlation measurement. As noise is added to the detector, this optimum aperture size increases to $3r_0$ for $\sigma = 3$ and $7r_0$ for $\sigma = 6$. With higher noise levels, no local minimum exists. This plot also shows that it is only at the smaller apertures that the noise affects tracking performance, reflecting the fact that for large aperture sizes the photon count overwhelms the detector noise. Thus the optimum aperture size for a noisy detector should be chosen based on fringe tracking rather than correlation measurement.

There is no clear optimum sample time for either the noiseless or noisy detector cases, although the longer the sample time the better the probability of fringe tracking. If too large a sample time is chosen, the fringe envelope can move significantly smearing out the peak in the channeled spectrum making fringe tracking impossible. The sample time should not be longer than 2-3 times τ_0 . If longer times are needed for faint objects longer integrations should be used. The paper by Lawson[9] contains a discussion of these problems.

6 Conclusion

High DQE noiseless detectors such as an APD will always have the best performance for both fringe tracking and correlation measurement. Unfortunately, these devices are not available in arrays and they have a high per-pixel cost. This work has shown that when choosing a detector that will allow fringe tracking on the faintest possible object with the lowest possible visibility and shortest possible sample time, a noisy high-DQE detector like a bare CCD becomes an attractive alternative, especially if the flexibility of on-chip rebinning is taken into account. It has also been shown that these devices can be used for correlation measurement although they only match the performance of a lower DQE noiseless array detector rather than improve on it. In the case of group delay tracking an optimum aperture size exists for a noisy detector and a method for calculating this has been given. In the case of sample times and correlation measurement no clear optimum were found and the optimum for a noiseless detector ($2.5r_0$ for aperture size and $1.6\tau_0$ for sample time) should be used.

CCDs with a readout noise figure of $\sigma = 6$ are now available, and it is to be hoped that noise levels of $\sigma = 3$ will be achieved on a production basis soon. Based on these calculations, a small low-noise CCD has a high enough DQE to make up for its readout noise making it a good detector for group delay tracking. Once in place it will also be possible to use this array detector for parallel correlation measurements in multiple spectral bands.

Acknowledgments

This work was supported by the Center for High Angular Resolution Astronomy at Georgia State University as part of the CHARA Array project. The CHARA Array is funded by the National Science Foundation through NSF grant AST-9414449 and by Georgia State University. I would also like to thank Peter Lawson for taking time to discuss the fringe tracking problem with me and his advice and code for calculating the integrals.

A Statistical methods

Both the signal term c_{ijk} and the noise term r_{ijk} follow standard statistical relationships. We will require terms up to and including the fourth moment. In the case of the signal c_{ijk} , which uses Poisson statistics, the following relationships apply

$$\begin{aligned}\langle c_{ijk}^2 \rangle &= \langle c_{ijk} \rangle^2 + \langle c_{ijk} \rangle \\ \langle c_{ijk}^3 \rangle &= \langle c_{ijk} \rangle^3 + 3\langle c_{ijk} \rangle^2 + \langle c_{ijk} \rangle \\ \langle c_{ijk}^4 \rangle &= \langle c_{ijk} \rangle^4 + 6\langle c_{ijk} \rangle^3 + 7\langle c_{ijk} \rangle^2 + \langle c_{ijk} \rangle.\end{aligned}\tag{48}$$

For the Gaussian noise process r_{ijk} , we have

$$\langle r_{ijk}^n \rangle = \begin{cases} (n-1)!! \sigma^n & \text{for } n \text{ even} \\ 0 & \text{for } n \text{ odd} \end{cases}\tag{49}$$

where we have used the standard notation

$$n!! = \begin{cases} 2 \times 4 \cdots \times n & \text{for } n \text{ even} \\ 1 \times 3 \cdots \times n & \text{for } n \text{ odd.} \end{cases}\tag{50}$$

We also note that the two parts, signal and noise, are statistically independent and so

$$\langle n_{ijk} \rangle = \langle c_{ijk} \rangle + \langle r_{ijk} \rangle\tag{51}$$

and

$$\langle c_{ijk}^n r_{ijk}^m \rangle = 0\tag{52}$$

for odd m .

In order to model the behaviour of a measurement system, we introduce a second form of average to be denoted by a line above a variable:

$$\overline{\langle n_{ijk} \rangle} = \frac{1}{M} \sum_{k=1}^{k=M} \langle n_{ijk} \rangle.\tag{53}$$

This is an average across many samples, that is, the atmosphere and OPD are free to move and will almost certainly have different values during different samples. The integration

time $M\tau$ is chosen such that the projected baseline does not change significantly and cause baseline smearing.

When analyzing a particular measurement system to find its expected value or some statistical moment, one must be careful to completely expand the expression in terms of the ensemble average first, using equations (48), (49), (51) and (52) and then analyze the time averaged statistics. This is equivalent to ensuring you know what is going on in a single sample before considering many samples.

To reduce the time averaged statistics we will need to consider moments of the cosine function. To do this we will assume the atmospheric term takes on a different and random value during each sample period and so

$$\begin{aligned} \overline{\cos^n \left(\frac{2\pi i}{P_\Phi} s_\Phi(\nu_j) + \frac{2\pi j}{P_\nu} s_\nu(k\tau) + \Phi(k\tau) \right)} &\approx \frac{1}{2\pi} \int_0^{2\pi} \cos^n x dx \\ &= \begin{cases} \frac{(n-1)!!}{n!!} & \text{for } n \text{ even} \\ 0 & \text{for } n \text{ odd.} \end{cases} \end{aligned} \quad (54)$$

As an example, we set out the SNR calculation for the known-noise Tango and Twiss estimator. We begin by calculating the variance of the unnormalised estimator using

$$\text{VAR}(\langle C_N^2 \rangle) = \frac{\text{VAR}(\langle q \rangle) + \text{VAR}(\langle \sum_{i=1}^4 n_i \rangle) - 2 \times \text{COVAR}(\langle q \rangle, \langle \sum_{i=1}^4 n_i \rangle)}{16N^2}. \quad (55)$$

Note that the division by $16N^2$ assumes that we know the value of N exactly, an assumption that has been made implicitly in all previously published SNR calculations. While this is not strictly true, it is a fairly good approximation provided that the number of samples in the measurement is relatively large.

The variances and covariances in equation (55) can then be calculated, being careful to full expand in terms of the ensemble average first and then the temporal average and we find that

$$\text{VAR}(\langle q \rangle) = 32N^3V^2 + 16N^2(1 + V^2) + 4N + 32\sigma^2(N^2V^2 + N) + 16\sigma^4, \quad (56)$$

$$\text{VAR}(\langle \sum_{i=1}^4 n_i \rangle) = 4N + 4\sigma^2 \quad (57)$$

and

$$\text{COVAR}(\langle q \rangle, \langle \sum_{i=1}^4 n_i \rangle) = 8N^2V^2 + 4N. \quad (58)$$

Combining equations (55), (56), (57) and (58) results in

$$\text{VAR}(\langle C_N^2 \rangle) = 2N^3V^2 + N^2 + \sigma^2(2N^2V^2 + 2N + \frac{1}{4}) + \sigma^4. \quad (59)$$

The SNR of a signal is the expected value divided by its standard deviation, and so we have

$$\text{SNR}(V^2) = \frac{\sqrt{M}N^2V^2}{\sqrt{2N^3V^2 + N^2 + \sigma^2(2N^2V^2 + 2N + \frac{1}{4}) + \sigma^4}}. \quad (60)$$

In order to compare this to other SNR expressions we recall that $N_{\Phi} = 4N$ in this system resulting in

$$\text{SNR}(V^2) = \frac{\sqrt{M}N_{\Phi}^2V^2}{4\sqrt{N_{\Phi}^2 + \frac{1}{2}N_{\Phi}^3V^2 + 8\sigma^2(\frac{1}{4}N_{\Phi}^2V^2 + N_{\Phi} + \frac{1}{2}) + 16\sigma^4}}. \quad (61)$$

References

- [1] N.S. Nightingale, “A New Silicon Avalanche Photodiode Photon Counting Detector for Astronomy,” *Experimental Astronomy*, **1(6)**, 407-422 (1991)
- [2] C. Papaliolios and L. Mertz, “New two-dimensional photon camera,” in *Instrumentation in Astronomy IV*, D.L. Crawford, ed, Proc. Soc. Photo-Opt, Instrum. Eng. **331**, 360-364 (1982)
- [3] P.R. Lawson, “Artifacts in PAPA Camera Images,” *Applied Optics*, **33**, 1146-1153 (1994)
- [4] J.W. Beletic, J.A. Zadnick, C.L. Tritsch and R.C. DuVarney, “Georgia Tech Low Light Level Imaging System,” in *SPIE Proc: High Resolution Imaging by Interferometry II*, Ed J.M. Beckers & F. Merkle (1991), pp. 12.
- [5] W.J. Tango and R.Q. Twiss, “Michelson Stellar Interferometry,” *Progress in Optics*, **Vol XVII**, 239 - 277 (1980)
- [6] D. Buscher, “Optimising a ground-based optical interferometer for sensitivity at low light levels,” *Mon. Not. R. astr. Soc.*, **235**, 1203-1226 (1988)
- [7] S.R. Kulkarni, S. Prasad and T. Nakajima, “Noise in Optical Synthesis Images. II. Sensitivity of an nC_2 Interferometer with Bispectrum Imaging,” *JOSA-A*, **8**, 499-510 (1991)
- [8] J.W. Beletic and R.M. Goody, “Recovery of Planetary Images by Speckle Imaging,” *Applied Optics*, **31**, 6909 - 6921 (1992)
- [9] P.R. Lawson, “Group delay tracking in optical stellar interferometry using the Fast Fourier Transform,” *JOSA-A*, **12**, 366-374 (1995)
- [10] J.W. Beletic, “Use of CCD Technology for Fringe Tracking in the CHARA Array,” Appendix P in *The CHARA Array: Final Report to the National Science Foundation*, (Report to NSF: Cooperative Agreement 90-08941, Atlanta, 1994)
- [11] H.A. McAlister et al, “The CHARA Array,” in *Proc: SPIE conference on Advanced Telescopes & Instrumentation*, 2200 (1994), pp. 129-139.
- [12] W.J. Tango & J. Davis, “Application of geometric phase techniques to stellar interferometry,” *Applied Optics*, **35**, 621 (1996)

- [13] T.A. ten Brummelaar, W.G. Bagnuolo Jr. & S.T. Ridgway, “Strehl ratio and visibility in long-baseline stellar interferometry,” *Optics Letters*, **20**, 521-523 (1995)
- [14] W.A. Traub, “Constant-dispersion grism spectrometer for channeled spectra,” *JOSA-A*, **7**, 1779-1791 (1990)
- [15] M. Shao et al, “The Mark III stellar interferometer,” *Astron. Astrophys*, **193**, 357-371 (1988)
- [16] J. Davis et al, “Progress in commissioning the Sydney University Stellar Interferometer (SUSI), ” in *Proc: SPIE conference on Advanced Telescopes & Instrumentation*, 2200 (1994), pp. 231-241.
- [17] J.F. Walkup and J.W. Goodman, “Limitations of fringe-parameter estimation at low light levels,” *J.O.S.A.* **63**, 399-407 (1973).
- [18] D.L. Fried, “Optical resolution through a randomly inhomogeneous medium for very long and very short exposures,” *JOSA*, **56**, 1372-1379 (1966)